Metasomatic Replacement of Albite in Nature and Experiments

Kirsten Drüppel [1],* and Richard Wirth [2]

[1] Institute of Applied Geosciences, Karlsruhe Institute of Technology (KIT), Adenauerring 20b, 76131 Karlsruhe, Germany

[2] Deutsches GeoForschungsZentrum, Telegrafenberg, 14473 Potsdam, Germany; wirth@gfz-potsdam.de

* Correspondence: kirsten.drueppel@kit.edu; Tel.: +49-721-608-43326

check for updates

Abstract: Replacement of albite by sodium-rich, secondary phases is a common phenomenon, observed in different geological settings and commonly attributed to alkaline metasomatism. We investigated growth of nepheline and sodalite on albite in time series experiments between two and 14 days. A total of 42 hydrothermal experiments were performed in cold-seal hydrothermal vessels at a constant pressure of 4 kbar and 200–800 °C in the system SiO_2–Al_2O_3–NaCl–H_2O. To allow for fluid flow and material transport, a double-capsule technique was used; hereby, a perforated inner Pt capsule was filled with cleavage fragments of natural albite, whereas the shut outer Au capsule was filled with γ-Al_2O_3 and the NaCl–H_2O solution. Complete overgrowth of albite by sodalite and nepheline occurred after just two days of experiments. At high salinity ($\geq$17 wt % NaCl) sodalite is the stable reaction product over the whole temperature range whereas nepheline occurs at a lower relative bulk salinity than sodalite and is restricted to a high temperature of $\geq$700 °C. The transformation of albite starts along its grain margins, cracks or twin lamellae. Along the reaction front sodalite crystallizes as small euhedral and highly porous grains forming polycrystalline aggregates. Coarse sodalite dominates in the outermost domains of the reaction zones, suggesting recrystallization. Sodalite may contain fluid inclusions with trapped NaCl-rich brine, demonstrating that the interconnected microporosity provides excellent pathways for fluid-assisted material transport. Highly porous nepheline forms large, euhedral crystals with rectangular outline. Sodalite and nepheline in natural rock samples display only minor porosity but fluid and secondary mineral inclusions, pointing to coarsening of a previously present microporosity. The reaction interface between sodalite and albite in natural rock samples is marked by open channels in transmission electron microscopy. In many of the experiments, a zone of Si–H-rich, amorphous material is developed at the reaction front, which occurs at a temperature of up to of 750 °C as nanometer to 350 μm wide reaction zone around albite. This change in composition corresponds with the abrupt termination of the crystalline feldspar structure. The presence of sodalite as micro- to nanometer-sized, euhedral crystals within the amorphous zone demonstrates, that both the sodalite reaction rim and the amorphous material allow for fluid-assisted material transport between the crystalline albite (release of Si, Al) and the bulk fluid (H_2O, Na, Cl). This texture, moreover, suggests that the amorphous phase represents a metastable interstage reaction product, which is progressively replaced by sodalite and nepheline. Remarkably, product sodalite, nepheline, and the amorphous material largely inherit the trace element budget of the respective ancestor albite, indicating that at least part of the trace elements remained fixed during the reaction process. The observed reaction textures in both natural and experimental samples indicate an interfacial dissolution–reprecipitation mechanism. Results of our study bear important implications with respect to mineral replacement in the presence of a fluid phase, especially regarding the interpretation of trace element patterns of the product phases.

1. Introduction

Replacement of a mineral by a more stable one is a widespread phenomenon in distinct geological environments and processes. This project focuses on the alkaline metasomatic transformation of albite in the presence of a NaCl-rich fluid phase. A major feature of this reaction type is material transport along grain and interphase boundaries in the hydrous fluids. When the reaction is completed the newly formed mineral had crystallized in the pre-existing volume of the ancestor mineral. In general, such mineral pseudomorphs preserve the external shape and accordingly the volume of the parent phase [1–6]. Another consequence of fluid–assisted mineral reactions, generally irrespective of the relative molar volumes of the parent and product phases, is the development of an interconnected microporosity in the product providing new pathways for circulating fluids [4,5,7,8]. The reaction produces a front between the educt and product phases. Despite the large number of studies concerning mineral replacement processes, the mechanisms involved are not fully understood. In part this is due to the complexity of natural mineral solid solutions and fluid compositions, when compared to common experimental setups. In addition, the physical and chemical conditions during the mineral replacement reaction in natural rocks are very difficult to estimate. Even if the peak P–T conditions of a rock can be calculated from geothermobarometry, it is often not clear at what stage and over what P–T interval pseudomorphs formed. In order to construct a replacement model, it is hence useful to combine microscopic observations and geochemical analyses of natural rock samples, for which the boundary conditions of the respective replacement reaction are known, with well-defined experimental investigations. This allows investigating experimentally the conditions under which a solid phase forms or changes as a function of the composition of the surrounding fluid and to further apply the results to more complex, natural systems.

The present experimental study explores growth of sodalite ($Na_8Al_6Si_6O_{24}Cl_2$), nepheline ($NaAlSiO_4$), and minor analcime ($NaAlSi_2O_6 \cdot H_2O$) on albite in the system SiO_2–Al_2O_3–NaCl–H_2O, mainly governed by dissolution, material transport from an external source and re-precipitation. In natural systems, these minerals typically occur in silica undersaturated igneous rocks such as nepheline syenites or alkali-metasomatized rocks. The chemical reactions describing these various transformations were proposed by [9] and then accepted by many scientists, e.g., [10–13]. According to observations of the alkali-metasomatic replacement of feldspars in experiments and natural metasomatic rock samples [9–14], experiments were performed at crustal pressures of 4 kbar, late-igneous to hydrothermal temperatures of 200–800 °C, and a fluid phase of variable salinity. We used a double-capsule technique, where an albite crystal, serving as source for Si, Na, and Al, is physically separated from γ-Al_2O_3 and material transport occurs via a H_2O–NaCl fluid. After identification of the run products with X-ray diffraction (XRD) and high-resolution scanning electron microscopy (SEM), the composition of the coexisting phases was determined by electron microprobe analysis (EMPA). Internal microstructures like porosity or open pathways for element transport were studied with SEM and transmission electron microscopy (TEM), using the focused ion beam (FIB) method. Of special interest was the geometry and nature of the reaction front to characterize a possible influence of pre-existing heterogeneities like grain boundaries and microcracks on its origin and evolution. These methods allowed identifying the preferred pathways of the metasomatic solutions. The timing, nature and distribution of micropores and microcracks were used to decide whether these structures preferentially form along specific crystallographic orientations in albite or if they are mainly controlled by the grain boundaries of the phases involved. In addition, we investigated the behavior of trace elements during the replacement of plagioclase with in situ laser ablation ICPMS (LA-ICPMS) analysis. The knowledge about redistribution patterns of elements—in our case the spatial distribution of Sr and the light

REE—may help to interpret trace and rare earth element data with respect to natural mineral-forming processes. General conclusions of this project can be applied to other synthetic and natural systems, where similar replacement textures are observed.

2. Materials and Methods

2.1. Starting Materials

Cleavage fragments of natural albite from Swartbooisdrif, Namibia, Lomnitz, Poland, and Lovozero, Russia were used as educt phases for the hydrothermal experiments. A detailed description and analyses of the starting material are given in Section 3.1.

2.2. Experimental Setup and Procedure

A total of 42 hydrothermal experiments were performed in the system SiO_2–Al_2O_3–NaCl–H_2O (P: 4 kbar, T: 200–800 °C, 2–14 days; Table 1) in a conventional hydrothermal apparatus with horizontally arranged, Tuttle-type cold-seal vessels. For all experiments, a double-capsule technique was used to allow for fluid mobility. Hereby, a shut but perforated inner platinum capsule of 2.5 mm in diameter was filled with weighed amounts of cleavage fragments of natural albite of 0.5–1.2 mm in diameter (4–5 pieces) from different localities (i.e., Swartbooisdrif, Namibia, Lomnitz, Poland, Lovozero, Russia), whereas the shut outer capsule was filled with γ-Al_2O_3 and an aqueous brine of varying salinity (Figure 1). These inner capsules were placed in a welded outer gold capsule of 4.6 mm in diameter, filled with γ-Al_2O_3 and a mixture of analytical grade NaCl and distilled H_2O with varying salinity (9–75 wt % NaCl) as starting materials. A minor amount of NaOH (0.2 mol/L) was added to the fluid in order to promote solubility and transport of silica. The mixture was loaded into an Au capsule, the perforated Pt capsule with albite was placed on top, then the Au capsule was sealed by arc welding. The experimental design allows the saline fluid to migrate between the two capsules, hence promoting fluid-assisted mass transfer between the inner and the outer capsule. The capsule was placed in an oven at 110 °C for 12 h to check for tightness and was then put in externally heated cold-seal vessels.
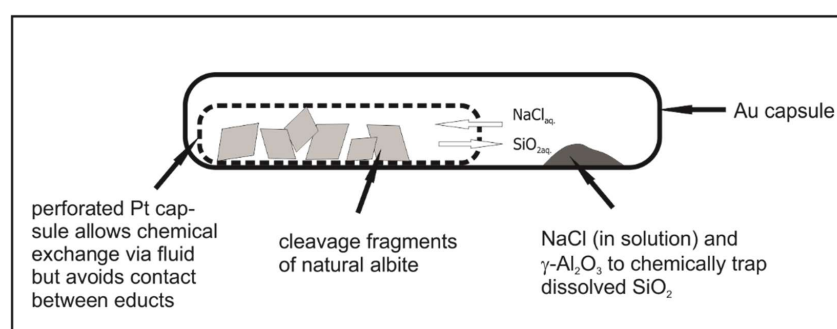

Figure 1. Experimental setup for the replacement of albite by sodalite and/or nepheline. The starting albite crystals are physically separated from γ-Al_2O_3 by a shut but perforated Pt capsule (2.5 mm in diameter), providing pathways for the bulk fluid, an H_2O–NaCl solution of variable salinity. Cleavage fragments of albite were in the order of 0.5–1.2 mm in diameter, the powdered γ-Al_2O_3 was placed in an outer Au capsule (4.6 mm in diameter) of approximately 2.5 to 3 cm in length (figure not to scale).

According to observations in natural rock samples, the vessels were pressurized by water to 4 kbar and heated under controlled pressure to 300–800 °C. The temperature during the experiments was controlled with NiCr-Ni thermocouples, with the temperature being accurate within ±5 °C. Fluid pressures were measured with Heise gauges with an estimated uncertainty of ±50 bar. The experiments were ended by switching off the power and cooling the autoclaves with compressed air to a temperature of <100 °C within 5 min, while maintaining the pressure.

Table 1. Starting materials, run conditions and products of hydrothermal experiments for the metasomatic transformation of albite to sodalite and nepheline.

Experiment	Starting Material	P (kbar)	T (°C)	d (days)	Salinity (wt %)	Solid Run Products
29	albite (Lomnitz), NaCl, -Al_2O_3	4	200	14	26	albite, halite, boehmite, sodalite
31	albite (Lomnitz), NaCl, -Al_2O_3	4	200	7	26	albite, halite, boehmite, sodalite
33	albite (Lomnitz), NaCl, -Al_2O_3	4	200	2	75	albite, halite, boehmite, sodalite, amorphous phase
13	albite (Lomnitz), NaCl, -Al_2O_3	4	300	6	39	albite, halite, corundum, boehmite, sodalite
20	albite (Lomnitz), NaCl, -Al_2O_3	4	300	7	39	albite, halite, corundum, boehmite, sodalite
LT-20	albite (Lomnitz), NaCl, -Al_2O_3	4	330	6	10	albite, halite, boehmite, analcime
LT-16	albite (Swartb.), NaCl, -Al_2O_3	4	350	6	17	albite, halite, boehmite, sodalite, analcime
LT-21	albite (Lomnitz), NaCl, -Al_2O_3	4	400	6	9	albite, halite, corundum, boehmite, analcime
07	albite (Swartb.), NaCl, -Al_2O_3	4	400	6	29	albite, halite, corundum, boehmite, sodalite
14	albite (Lomnitz), NaCl, -Al_2O_3	4	400	6	38	albite, halite, corundum, boehmite, sodalite, amorphous phase
LT-17	albite (Swartb.), NaCl, -Al_2O_3	4	450	6	17	albite, halite, corundum, boehmite
LT-02	albite (Swartb.), NaCl, -Al_2O_3	4	450	6	35	albite, halite, corundum, boehmite, sodalite, analcime
LT-05	albite (Swartb.), NaCl, -Al_2O_3	4	450	6	50	albite, halite, corundum, boehmite, sodalite
LT-22	albite (Lomnitz), NaCl, -Al_2O_3	4	500	6	9	albite, halite, corundum, boehmite
09	albite (Lomnitz), NaCl, -Al_2O_3	4	500	7	32	albite, halite, corundum, boehmite, sodalite, analcime, amorphous phase
LT-12	albite (Swartb.), NaCl, -Al_2O_3	4	550	6	15	albite, halite, corundum
LT-18	albite (Swartb.), NaCl, -Al_2O_3	4	550	6	17	albite, halite, corundum, boehmite
01	albite (Lovoz.), NaCl, -Al_2O_3	4	550	6	27	albite, halite, corundum
LT-03	albite (Swartb.), NaCl, -Al_2O_3	4	550	6	35	albite, halite, corundum, sodalite
15	albite (Lomnitz), NaCl, -Al_2O_3	4	550	6	39	albite, halite, corundum, sodalite
LT-04	albite (Swartb.), NaCl, -Al_2O_3	4	550	6	51	albite, halite, corundum, sodalite
10	albite (Lomnitz), NaCl, -Al_2O_3	4	600	7	25	albite, halite, corundum, sodalite
HT-10	albite (Lovoz.), NaCl, -Al_2O_3	4	600	6	30	albite, halite, corundum, sodalite
18	albite (Lomnitz), NaCl, -Al_2O_3	4	600	7	39	albite, halite, corundum, sodalite, amorphous phase
05	albite (Swartb.), NaCl, -Al_2O_3	4	600	6	41	albite, halite, corundum, sodalite
HT-12	albite (Lomnitz), NaCl, -Al_2O_3	4	600	6	42	albite, halite, corundum, sodalite
16	albite (Lomnitz), NaCl, -Al_2O_3	4	650	6	39	albite, halite, corundum, sodalite, amorphous phase
HT-08	albite (Lovoz.), NaCl, -Al_2O_3	4	650	6	44	albite, halite, corundum, sodalite
HT-04	albite (Lovoz.), NaCl, -Al_2O_3	4	650	6	55	albite, halite, corundum, sodalite
30	albite (Lomnitz), NaCl, -Al_2O_3	4	700	14	17	albite, halite, corundum, nepheline, amorphous phase
HT-13	albite (Lovoz.), NaCl, -Al_2O_3	4	700	6	17	albite, halite, corundum, nepheline
HT-11	albite (Lovoz.), NaCl, -Al_2O_3	4	700	6	27	albite, halite, corundum, sodalite, nepheline
34	albite (Lomnitz), NaCl, -Al_2O_3	4	700	2	28	albite, halite, corundum, sodalite, nepheline, analcime, amorphous phase
32	albite (Lomnitz), NaCl, -Al_2O_3	4	700	7	29	albite, halite, corundum
11	albite (Lomnitz), NaCl, -Al_2O_3	4	700	7	31	albite, halite, corundum, sodalite, amorphous phase
HT-14	albite (Lomnitz), NaCl, -Al_2O_3	4	700	6	34	albite, halite, corundum, sodalite
04	albite (Swartb.), NaCl, -Al_2O_3	4	700	6	42	albite, halite, corundum, sodalite, nepheline
HT-15	albite (Lovoz.), NaCl, -Al_2O_3	4	700	6	43	albite, halite, corundum, sodalite
HT-16	albite (Lovoz.), NaCl, -Al_2O_3	4	700	6	44	albite, halite, corundum, sodalite
12	albite (Lomnitz), NaCl, -Al_2O_3	4	750	7	40	albite, halite, corundum, sodalite, analcime, amorphous phase
HT-09	albite (Lovoz.), NaCl, -Al_2O_3	4	750	6	49	albite, halite, corundum, sodalite
HT-02	albite (Lovoz.), NaCl, -Al_2O_3	4	800	6	42	albite, halite, corundum, sodalite, nepheline
HT-06	albite (Lovoz.), NaCl, -Al_2O_3	4	800	6	62	albite, halite, corundum, sodalite

2.3. Analysis of the Solid Run Products

Characterization of the initial and experimental product phases was performed with several analytical and imaging methods. XRD patterns for powders of synthesis products were obtained by a PHILIPS PW 1050 diffractometer (Philips Analytical, Almelo, The Netherlands) with Bragg-Brentano geometry and a scintillation counter, using Ni-filtered CuKα radiation (40 kV, 30 mA) housed at the department of applied Geosciences, Technical University of Berlin, Germany. Phase analysis was carried out with PHILIPS X´Pert Plus 1.0 (1999).

Reaction textures were investigated with a high-resolution SEM (Type Hitachi S-4000, Tokyo, Japan), housed at the Center of Electron Microscopy (ZELMI), Technical University of Berlin, Germany. For qualitative investigations with the SEM, the solid run products were dispersed on a carbon-coated sample carrier and sputtered with gold. For detailed investigation of the reaction front and the microstructures, polished thin sections were prepared and investigated under back-scattered electron (BSE) mode. Semi-quantitative analyses of the compositions of the solid run products were performed with a conventional SEM (Type Hitachi S-2700, Tokyo, Japan), equipped with an Energy Dispersive Spectrometer (EDS) on polished, carbon-coated thin sections.

EMPA (Cameca, Gennevilliers, France) of the compositions of the educt and product phases was performed on a Cameca Camebax instrument at the ZELMI, TU Berlin, Germany. Natural and synthetic standards were used for instrument calibration. Mineral analyses were performed with an accelerating voltage of 15 kV, a beam current of 20 nA and an electron beam of 5 μm in diameter.

In situ LA-ICPMS trace element analyses of the initial albite and product phases of the hydrothermal experiments were performed to investigate the behavior of trace elements during metasomatism. The thin sections were analyzed with a 266 nm Nd:YAG laser (New Wave Research Inc., Merchantek Products, Fremont, CA, USA) connected to a quadrupole ICPMS (Agilent 7500i; Plasma power: 1320 W; Carrier gas flow: 1.11 L·min^{-1} (Ar); Plasma gas flow: 14.9 L·min^{-1} (Ar); auxiliary gas flow: 0.9 L·min^{-1} (Ar)) at the Institute of Mineralogy, Würzburg. Laser parameters used were a frequency of 10 Hz and an energy setting of 50% (0.9 mJ). Ablation patterns were 600 μm long lines, ablated with a scan speed of 10 μm/s. The diameter of the sample pit created by the laser is 50 μm. Data acquisition was done in time-resolved analysis mode with measurements of the instrument background (20 s) and of sodalite, albite, nepheline, and amorphous material (60 s). The certified reference material NIST 612 with the values of [15] was used as an external standard, whereas Si in albite and its replacement products, derived from the electron microprobe analyses, was used as internal standard. Raw counts for each element were solely corrected by subtracting the background counts and processed using the software GLITTER (Version 3.0; On-line Interactive Data Reduction for the LA-ICPMS, Macquarie Research Ltd., Sydney, Australia, 2000).

The geometry and nature of the reaction front were investigated by high-resolution TEM (FEI company, Hillsboro, OR, USA) at the GeoForschungsZentrum Potsdam (GFZ). Electron transparent foils for TEM were cut from selected areas across the reaction fronts in the naturally and experimentally reacted albite in polished thin sections by focused ion beam (FIB) milling in an ultra-high vacuum using a FEI FIB200 instrument (FEI Company, Hillsboro, OR, USA, see [16,17] for details). TEM investigations were performed on a FEI Tecnai G2 F20 X-Twin system incorporating a field-emission electron gun (operated at 200 kV), a Fishione high-angle annular dark-field detector (HAADF), a Gatan Tridiem imaging filter for acquisition of energy-filtered images and electron energy-loss spectroscopy (EELS) element mapping, and an EDAX Genesis X-ray analyzer with an ultrathin window. Characterization of the reaction front in natural and reacted samples included bright-field and dark-field imaging, and EDX analyses (in scanning-TEM mode).

3. Results

3.1. Composition of the Starting Materials

Cleavage fragments of natural albite of 0.5–1 mm in size comprise (1) metasomatic albite from Swartbooisdrif, Namibia; (2) fissure-grown albite from Lomnitz, Poland; and (3) fissure-grown albite from Lovozero, Russia. Namibian albite is the main mineral of a sodium-rich fenite, containing minor ankerite, sodalite, magnetite, and biotite. Albite is subhedral and microscopically clear, but may contain rare inclusions of biotite. Individual albite grains are up to 0.5 cm in size. Many albite grains do not display polysynthetic twin lamellae but, if present, twinning is on the albite law. Fissure-grown albites from both Poland and Russia form euhedral and glass-clear crystals. Poland albite is up to 1.5 cm in size and associated by calcite and quartz whereas medium-grained albite (1–5 mm) from Russia has grown as a grass-like crystal layer on alkali feldspar. Both albite types are unweathered and frequently twinned on the albite law.

The chemical composition of the different albites was determined by EMP analysis, averaging analyses from profiles of 10 to 15 points. Albite from all different localities is almost pure, homogeneous albite ($Ab_{99–100}$), with CaO, MgO, FeO, K_2O, and BaO contents at or below the detection limit (Table 2). Only minor Swartbooisdrif albite may show elevated Ca contents of up to 1 wt % (Ab_{95}). The three different albites differ regarding their trace element composition, analyzed by La-ICPMS (Table A1). Concentrations in Ca and Sr are highest in the Swartbooisdrif and lowest in the Lovozero albite, whereas Ba, Sc, Mn, Co, Ti, and the LREE contents decrease from Swartbooisdrif over Lovozero towards Lomnitz albite, the latter of which having LREE contents below the detection limit. Concentrations of Zn, Ga, Cu, and Y are highest in the Lovozero albite. Contents of the HREE (Gd to Lu) are below the detection limit in all samples.

Table 2. Representative EMP analyses of educt albite from Lomnitz, Lovozero, and Swartbooisdrif.

Sample	29	30	31	33	34	HT-08	HT-09	HT-10	LT-05	LT-07
Point	23	28	30	18	7	13	23	47	63	79
Mineral	albite Lomnitz	albite Lomnitz	albite Lomnitz	albite Lomnitz	albite Lomnitz	albite Lovozero	albite Lovozero	albite Lovozero	albite Swartb.	albite Swartb.
Analysis					wt %					
SiO_2	68.5	68.4	68.7	68.5	68.3	68.6	68.8	68.7	67.1	68.6
Al_2O_3	20.2	20.6	20.2	20.0	19.7	19.8	20.5	20.3	21.9	19.5
Fe_2O_3	0.05	0.00	0.00	0.00	0.03	0.01	0.04	0.01	0.04	0.02
CaO	0.02	0.05	0.06	0.02	0.02	0.02	0.01	0.00	0.99	0.02
Na_2O	11.4	11.5	11.7	11.6	11.3	12.2	12.4	11.7	10.8	12.2
K_2O	0.01	0.03	0.04	0.03	0.04	0.04	0.17	0.06	0.55	0.03
BaO	0.00	0.01	0.00	0.01	0.00	0.01	0.00	0.00	0.01	0.00
Sum	100.1	100.6	100.7	100.1	99.4	100.6	101.8	100.8	101.4	100.3

3.2. Experimental Run Products and Replacement Textures

A total of 42 hydrothermal experiments were performed in the system SiO_2–Al_2O_3–NaCl–H_2O (P: 4 kbar, T: 200–800 °C, 2–14 days) to provide a better understanding of the reaction processes related to the alkali-metasomatic replacement of albite. Run conditions, composition of the solid starting materials and salinities of the fluid phase are listed in Table 1. The replacement of albite never went to completion, so albite remained present in all experiments.

At high salinity sodalite was found to be the stable phase over the whole temperature range (Figure 2). As temperature rises, more NaCl is needed to stabilize sodalite. Nepheline occurred at a temperature >700 °C and lower average bulk salinity of the fluid. Remarkably, there is a discontinuity in the occurrence of nepheline in experiments performed at 700–800 °C. At 700 °C, the feldspathoid is observed at salinities of 17–28 wt % NaCl, then disappears, and appears again at a salinity of 42 wt % NaCl. It is not observed in experiments performed at 750 °C but in experiment HT-02 at 800 °C, 42 wt % NaCl.

Even during the shortest experiment of two days, complete overgrowths of sodalite and nepheline occurred on albite. Analcime is present as a minor phase in many of the experiments (at variable salinities of 9–40 wt % NaCl), where it forms part of the replacement assemblage in the inner capsule. In the outer capsule, originally filled with γ-Al$_2$O$_3$ and an aqueous brine of varying salinity, boehmite is preserved at low temperature, whereas corundum is found at T ≥ 550 °C. Nepheline exclusively grew around albite in the inner capsule and was not detected outside the inner capsule. Euhedral, isolated sodalite, on the other hand, is also frequently present in the outer capsule at high bulk salinity, testifying to transport of silica via the aqueous brine and its reaction with γ-Al$_2$O$_3$. Representative EMP analyses of the educt albite and the product phases of sodalite, nepheline, and analcime are listed in Tables 2 and 3, respectively.
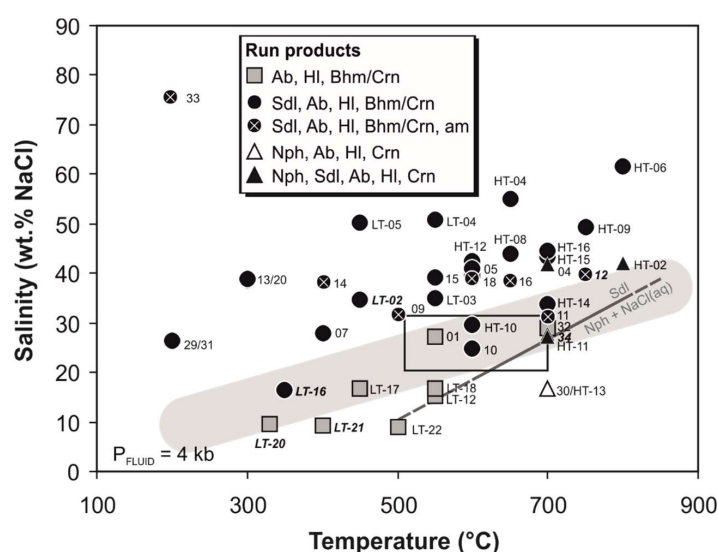

Figure 2. Salinity vs. temperature diagram for run products of the hydrothermal experiments. Rectangle marks the temperature and salinity conditions calculated for natural, sodalite-bearing rock samples of Namibia [18,19]. Samples marked bold-italic additionally contain analcime as reaction product. Grey solid and stippled line marks the experimentally derived course of the reaction 6 nepheline + 2NaCl(aq) = sodalite after [14]. Grey shaded area marks approximate course of the metasomatic replacement of albite by sodalite, following the reaction 6 albite + 2NaCl(aq) = sodalite + 12SiO$_2$(aq). (*Ab* albite, *Bhm* boehmite, *Crn* corundum, *Hl* halite, *Nph* nepheline, *Sdl* sodalite).

Table 3. Representative EMP analyses of product sodalite, nepheline, and analcime.

Sample	10	34	HT-04	HT-08	HT-10	LT-04	LT-05	LT-06	LT-07	LT-07	30	34	34	HT-11	HT-13	12	34	34
Point	16	14	8	16	48	59	66	68	78	80	27	3	8	35	31	8	10	11
Mineral					sodalite								nepheline				analcime	
Analysis									wt %									
SiO$_2$	38.3	36.6	37.5	37.2	37.1	37.1	37.7	38.0	37.7	37.1	47.8	49.9	47.4	46.5	40.7	56.8	55.3	55.0
Al$_2$O$_3$	30.5	31.8	32.7	32.6	32.0	32.3	32.4	31.7	32.5	32.5	34.6	32.3	33.1	34.0	35.9	23.1	25.9	26.0
Fe$_2$O$_3$	0.02	0.00	0.05	0.00	0.02	0.11	0.00	0.03	0.00	0.00	0.04	0.03	0.00	0.05	0.00	0.07	0.00	0.04
CaO	0.03	0.02	0.00	0.04	0.00	0.07	0.04	0.22	0.04	0.01	0.07	0.04	0.04	0.00	0.04	0.07	0.01	0.00
Na$_2$O	24.9	24.7	25.8	25.2	26.0	25.0	24.8	23.7	25.8	26.0	18.9	18.2	19.2	19.6	22.7	11.9	10.4	9.3
K$_2$O	0.00	0.00	0.07	0.14	0.18	0.05	0.06	0.06	0.07	0.08	0.05	0.01	0.00	1.29	1.63	0.02	0.02	0.05
Cl	9.15	8.66	6.30	6.41	6.27	6.30	6.36	6.26	6.11	6.17	0.00	0.02	0.00	0.02	0.15	0.41	0.37	0.34
Sum	102.8	101.8	102.4	101.6	101.6	101.0	101.3	100.0	102.2	101.9	101.4	100.5	99.8	101.4	101.1	92.3	91.9	90.7

The transformation of albite to sodalite starts along the grain margins and, if present, along cracks (Figure 3a) and propagates until a complete pseudomorph of sodalite after albite has formed. The product sodalite forms euhedral crystals, in short experiments displaying a pseudohexagonal shape due to fast growth (Figure 3b). Along the embayed reaction fronts sodalite crystallizes

as very fine grained, highly porous grains forming polycrystalline aggregates with randomly oriented crystallites. Larger grains of massive sodalite dominate in the outermost domains of the reaction zones (Figure 3c), suggesting coarsening of early sodalite aggregates. An increasing run duration also involves coarsening of the grains, resulting in formation of massive sodalite along the reaction front. If present, albite twin lamellae are preferentially dissolved during the reaction process. Hereby, the reaction zones propagate from twin planes towards the center of individual lamellae. Polycrystalline sodalite aggregates partially fill the former lamellae but display no detectable crystallographic relationship with albite (Figure 3d). Along the outermost margins of the reaction rim, euhedral sodalite grew into the fluid and newly nucleated sodalite grains occur on the surfaces of previously crystallized sodalite even after long run times of 14 days. This texture indicates fluid transport through the sodalite rim and immediate reaction at the sodalite–fluid interface. Newly formed sodalite is often extremely porous (Figure 3e) with the interconnected microporosity providing excellent pathways for fluid-assisted material transport from and towards the reaction front. In five of the 42 experiments, sodalite contains numerous fluid inclusions, containing the trapped NaCl-rich aqueous fluid.
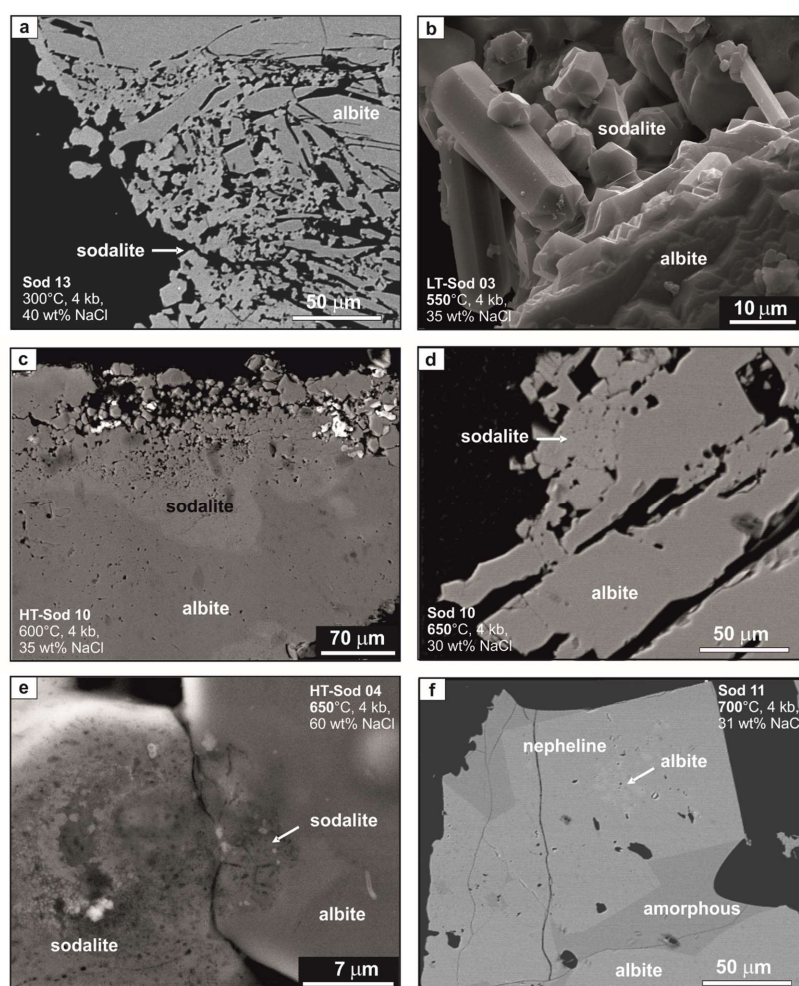

Figure 3. Reaction textures during the metasomatic replacement of albite (SEM images). (**a**) Sodalite replacing albite along the grain margins and cracks; (**b**) Hexagonal sodalite prisms, formed due to fast growth of sodalite; (**c**) Embayed reaction front with sodalite replacing albite; (**d**) Sodalite replacing albite along twin lamellae; (**e**) Sodalite is characterized by a high microporosity; (**f**) Nepheline crystals with rectangular outline replace albite at a high temperature of >650 °C.

At lower salinities of the fluid and a temperature of >700 °C, nepheline forms at the expense of albite. Like sodalite, nepheline displays a high porosity but, in contrast to sodalite, forms large, crystals with rectangular outlines of up to 150 μm in length that do not display any pseudomorphic relationship with the ancestor albite (Figure 3f). Small irregular patches of the original albite are preserved as inclusions in the newly formed nepheline.

3.3. Amorphous Material Formation

A conspicuous feature in many of the experiments is a zone of amorphous material, which developed at the reaction front between albite and newly formed sodalite and/or nepheline (Figure 4). The highly porous amorphous material is present during every stage of the experiments and at almost every experimental condition (even up to a temperature of 750 °C) as several nanometers to 350 μm wide reaction zone around albite relicts, separating it from sodalite and nepheline. A reaction rim of polycrystalline sodalite aggregates surrounds the amorphous material (Figure 4a,b). In extreme cases, the amorphous material may form an almost complete pseudomorph after albite (Figure 4b). Numerous cracks in the amorphous material point to a gel-like nature and high amounts of volatiles before cooling and drying of the samples (Figure 4a–c). Investigation with TEM reveals that the reaction interface between both sodalite and albite and the amorphous material is always sharp. Occasionally, an open channel is developed between albite and the amorphous zone, suggesting a structural discontinuity and lack of adhesion between the two phases; this channel may be filled by precipitates of the migrating fluid (i.e., mainly NaCl; Figure 4e,f). When compared to the ancestor albite, the amorphous layer is uniformly depleted in Na and, to a minor degree, in Al and enriched in Si and H. Chlorine contents are close to or below the detection limit. The drastic change in composition at the boundary with the amorphous layer corresponds with the abrupt termination of the crystalline feldspar structure. The presence of sodalite as micro- to nanometer-sized, euhedral crystals and diffuse Schlieren in the amorphous matrix is indicative of in situ nucleation and growth (Figure 4c,d). Their formation, however, requires transport of Al of the crystalline albite and migration of the NaCl-rich aqueous fluid into the Si-rich amorphous layer and suggests that material transport via the fluid phase is the most important process of this reaction type.

3.4. Behavior of Trace Elements during Replacement

To investigate the behavior of trace elements during metasomatism, albite from three different localities (Swartbooisdrif, Namibia, Lomnitz, Poland, Lovozero, Russia) each of which displaying its own characteristic trace element pattern, were used as educt phases. Remarkably, both the product sodalite and nepheline as well as the amorphous material inherit the trace element budget of the respective albite, displaying similar trace element patterns (Figure 5, Tables A1 and A2). Following this, the trace element contents of the solid product phase are mainly controlled by the bulk trace element budget of the reacting phase and not by fluid–mineral fractionation coefficients. It can be concluded that at least part of the trace elements remained fixed in the amorphous phase during the reaction process.
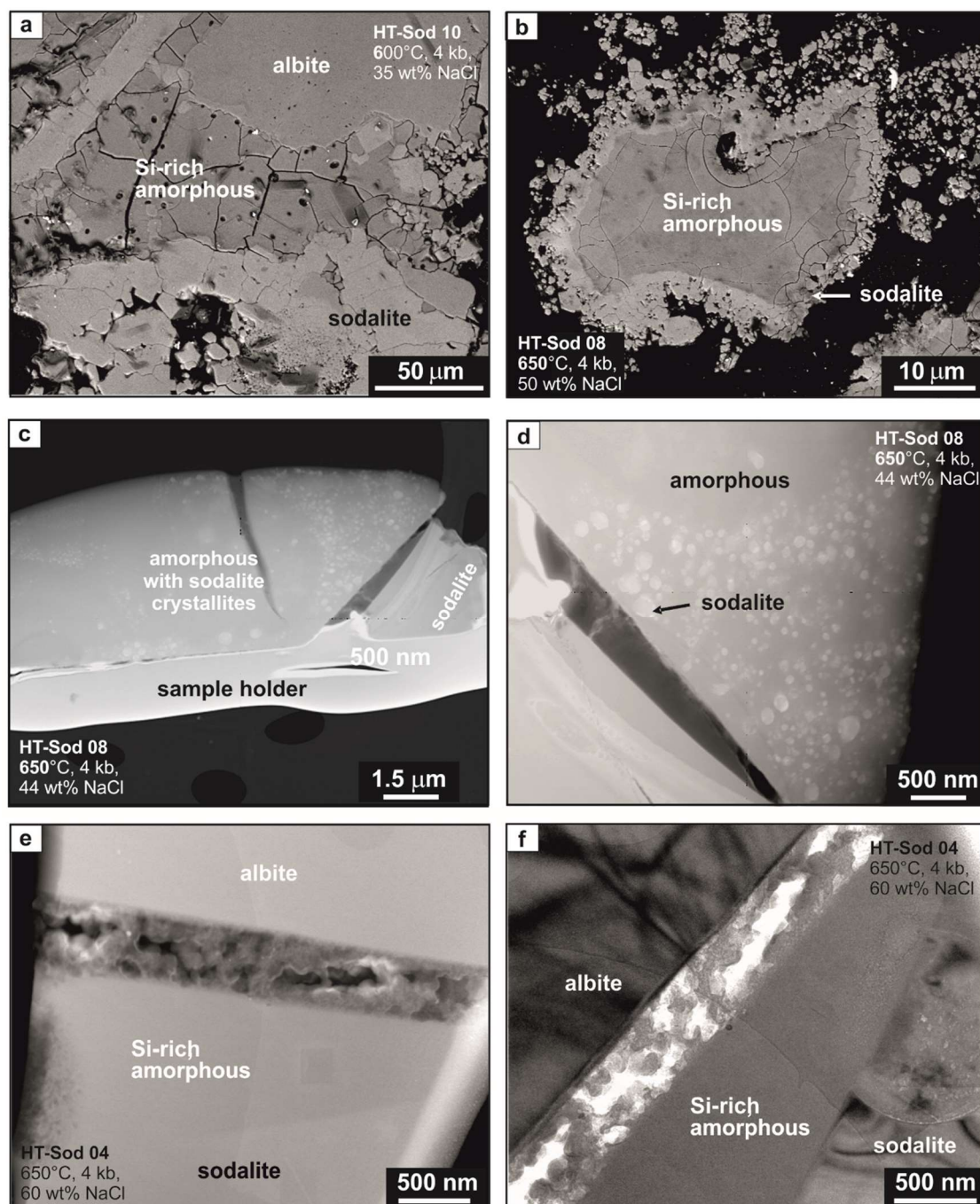
Figure 4. Amorphous material formation (**a**,**b**: SEM images; **c**–**f**: TEM images). (**a**) Amorphous material formation at the reaction front between albite and newly formed sodalite; (**b**) Amorphous material pseudomorphing the shape of former albite surrounded by newly formed sodalite; (**c**) TEM foil of the interphase boundary between sodalite and the amorphous phase in (**b**); A sharp contact is developed between sodalite and the amorphous material. Sodalite crystallization occurs irregularly, both within sharply defined areas and irregular Schlieren; (**d**) Detail of (**e**); (**e**) TEM foil of the interphase boundary between the educt albite and the newly formed sodalite separated by an open channel filled with NaCl crystals and a broad zone of Si-rich amorphous material; (**f**) Bright field image of (**e**).
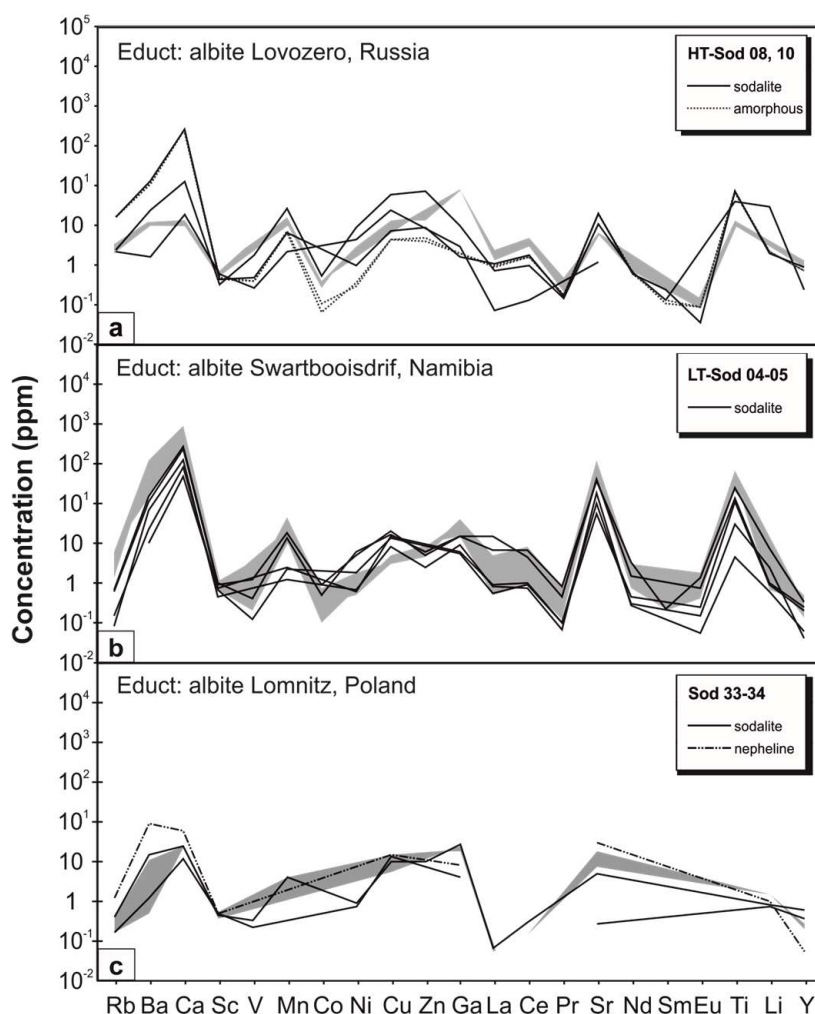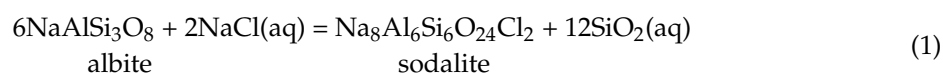
Figure 5. Laser-ICP-MS data for selected trace elements of different samples of educt albite (grey area) and the corresponding product sodalite, nepheline, and amorphous material of the hydrothermal experiments. (**a**) Experiments with fissure-grown albite from Lovozero, Russia; (**b**) Experiments with metasomatic albite from Swartbooisdrif, Namibia; (**c**) Experiments with fissure-grown albite from Lomnitz, Poland.

4. Discussion

4.1. Reaction Textures in the Experiments

Our hydrothermal experiments at 4 kbar, 200–800 °C in the system SiO_2–Al_2O_3–$NaCl$–H_2O show that albite is replaced by sodalite as the stable reaction product over the whole temperature range at high salinity, following Equation (1).

$$6NaAlSi_3O_8 + 2NaCl(aq) = Na_8Al_6Si_6O_{24}Cl_2 + 12SiO_2(aq) \tag{1}$$
$$\text{albite} \qquad\qquad\qquad \text{sodalite}$$

The formation of nepheline replacing albite (Equation (2)) occurs at high temperature but lower average bulk salinity of the fluid, also leading to an increase of Si in the solution.

$$NaAlSi_3O_8 = NaAlSiO_4 + 2SiO_2(aq) \tag{2}$$
$$\text{albite} \qquad \text{nepheline}$$
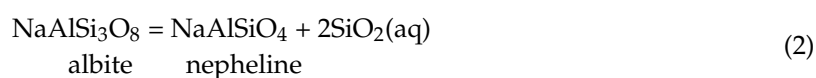
In part of the experiments (T: 700–800 °C, salinity: 27–42 wt % NaCl), both nepheline and sodalite were formed. In natural rock samples, the feldspathoids commonly display a replacement relationship (see Section 4.3), indicating progress of Equation (3).

$$6NaAlSiO_4 + 2NaCl \text{ (aq)} = Na_8Al_6Si_6O_{24}Cl_2$$

nepheline   sodalite   (3)
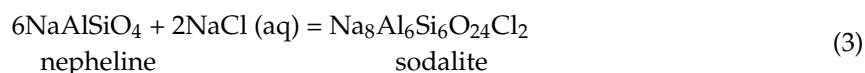
The fact that nepheline occurs discontinuously in the temperature-salinity range of the experiments may indicate, that part of the nepheline represents an interstage product, which is preserved or not, depending on the completion of the reaction. Textural relationships observed in our experiments, however, indicate that nepheline and sodalite rather coexist in this temperature-salinity interval, forming small, euhedral grains, crystallizing next to each other. This interpretation is in agreement with the experimental results of [14], who also observed a transition zone at intermediate salinities, where sodalite and nepheline coexist.

Analcime is a minor phase mainly present in experiments performed at low temperature <500 °C but also occurs as texturally late, accessory phase at temperatures of 700–750 °C, possibly formed during cooling. It commonly replaces albite, as in Equation (4).

$$NaAlSi_3O_8 + H_2O = NaAlSi_2O_6 \cdot H_2O + SiO_2\text{(aq)}$$

albite   analcime   (4)
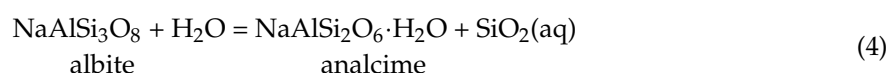
Equations (1), (2) and (4) demonstrate, that the dissolution of albite leads to a strong enrichment of Si in the solution. While the dissolved silica will be removed from the system in natural examples of metasomatism, in the experiments it remains in the system and progressively reacts with Al and Na to give nepheline, sodalite, and minor analcime.

A complete overgrowth of sodalite or nepheline on albite already occurred after two days, given the physicochemical conditions suitable for their formation. With increasing duration of the experiment (up to 14 days), the educt albite is increasingly consumed. Sodalite crystallizes as very fine grained, highly porous grains forming polycrystalline aggregates with randomly oriented crystallites displaying no detectable crystallographic relationship with albite, whereas nepheline forms large, euhedral crystals with rectangular outline. Both sodalite and nepheline are highly porous and may contain fluid inclusions with trapped NaCl-rich brine, demonstrating that the interconnected microporosity provides excellent pathways for fluid-assisted material transport.

A conspicuous feature of many of the experiments is a zone of highly porous, amorphous material, which occurs up to a temperature of 750 °C. If present, the amorphous material developed at the reaction front, ranging from several nanometers to a 350-μm reaction zone around albite. When compared to the latter, the amorphous layer is uniformly depleted in Na and Al and enriched in Si and H. This change in composition corresponds with the abrupt termination of the crystalline feldspar structure. The presence of sodalite as euhedral, micro- to nanometer-sized, euhedral crystals within the amorphous zone is indicative of its in situ nucleation and growth. Remarkably, both product sodalite and the amorphous material largely inherit the trace element budget of the respective ancestor albite, displaying almost indistinguishable trace element patterns, hence indicating that at least part of the trace elements remained fixed during the reaction process.

4.2. The Role of the Amorphous Phase

Amorphous layers, mainly developed between the fluid–solid interface and the unaltered mineral, are a common phenomenon of plagioclase alteration experiments under atmospheric conditions, in particular weathering experiments at acid to neutral pH [20–23]. Like the amorphous material developed in our alteration experiments, these near-surface amorphous regions are enriched in Si and H and show depletion in other metals, in particular the interstitial cations and Al [20–24]. The origin of the amorphous layer has been a subject of research and debate for years. It has been discussed in

terms of preferential leaching of cations due to differences in bond strength (i.e., nonstoichiometric dissolution) and interdiffusion with H$^+$ [25]. In recent years, authors have shown that the composition and nature of the amorphous material analyzed in their samples cannot be explained by a volume diffusion process but could be modeled assuming an interfacial dissolution–precipitation process (i.e., [24,26,27]). The findings in our experiments support the latter hypothesis. The sharp chemical and structural interface between albite and the amorphous layer, observed in our experiments, and the lack of albite structure relicts in the amorphous material indicates, that the latter represents an individual phase rather than a surface altered zone controlled by interdiffusion, like a leached layer. Following this, elements released from the albite structure (i.e., Si, Al, Na) may precipitate directly at the reaction front, forming a metastable reaction product, e.g., a hydrated silica gel. The fact that sodalite and nepheline (both NaCl-rich) subsequently crystallize in situ from the Si-rich and Na- and Al-poor amorphous material demonstrates that neither the outermost sodalite reaction rims nor the amorphous zone act as protective layers but allow for transport of aqueous chemical reactants and products between the crystalline reaction front (release of Si) and the bulk fluid (H$_2$O, Na, Cl, Al). Our findings are in agreement with an interface-coupled dissolution-precipitation model (see [6], for a review). The observation of sodalite and nepheline nucleating and growing within the amorphous layer strongly suggests that the amorphous layer represents a metastable intermediate phase rather than a final reaction product. Presumably, the amorphous material would have reacted with excess alumina and NaCl in the capsule to give sodalite and nepheline and be consumed if the experiment duration had been longer.

4.3. Reaction Textures in Natural Metasomatic Rock Samples

The replacement textures and chemical signatures of the run products of the experiments are remarkably similar to those of natural metasomatic rock samples. In natural fenite samples from NW Namibia, sodalite formed at the expense of anorthosite plagioclase during the subsolidus stage [18]. Alkali metasomatism occurred as a result of the interaction of anorthosites with sodium-rich, carbonatite-derived fluids. Mineral equilibria combined with fluid inclusions data prove that sodalite formed at c. 4 kbar and c. 700 $\pm$ 70 °C [18]. In syenites, also bordering the carbonatites, albite was progressively replaced by nepheline, followed by the formation of texturally late sodalite and cancrinite. The sodalitization of nepheline in the nepheline syenite occurred under a similar temperature (c. 775–700 °C) like the formation of sodalite overgrowth on albite [19]. The SiO$_2$-undersaturated bulk compositions of both the metasomatized anorthosites and syenites provide evidence that fenitization included removal of silica. While in nature, silica is removed from the system, in the experiments silica cannot be removed and reacts with alumina and Na to give nepheline, sodalite, and minor analcime.

The texture of syenites neighboring carbonatite at Swartbooisdrif, NW Namibia, is inhomogeneous with fine-grained K-feldspar-rich zones alternating with irregular zones, mainly composed of nepheline crystals of up to 5 cm in length, preserving numerous albite inclusions. At the direct contact to the carbonatite dykes pegmatoidal, euhedral nepheline crystals of up to 15 cm across can be observed (Figure 6a), which are virtually free of albite inclusions. The increase of the nepheline crystal size at the contact to the carbonatite dyke and the replacement of nepheline by sodalite may be attributed to the late influx of Na-rich carbonatitic fluids, triggering nepheline growth. In these zones, nepheline exhibits a pale blue tint, from its partial replacement by sodalite along grain margins and irregular cracks (Figure 6b).
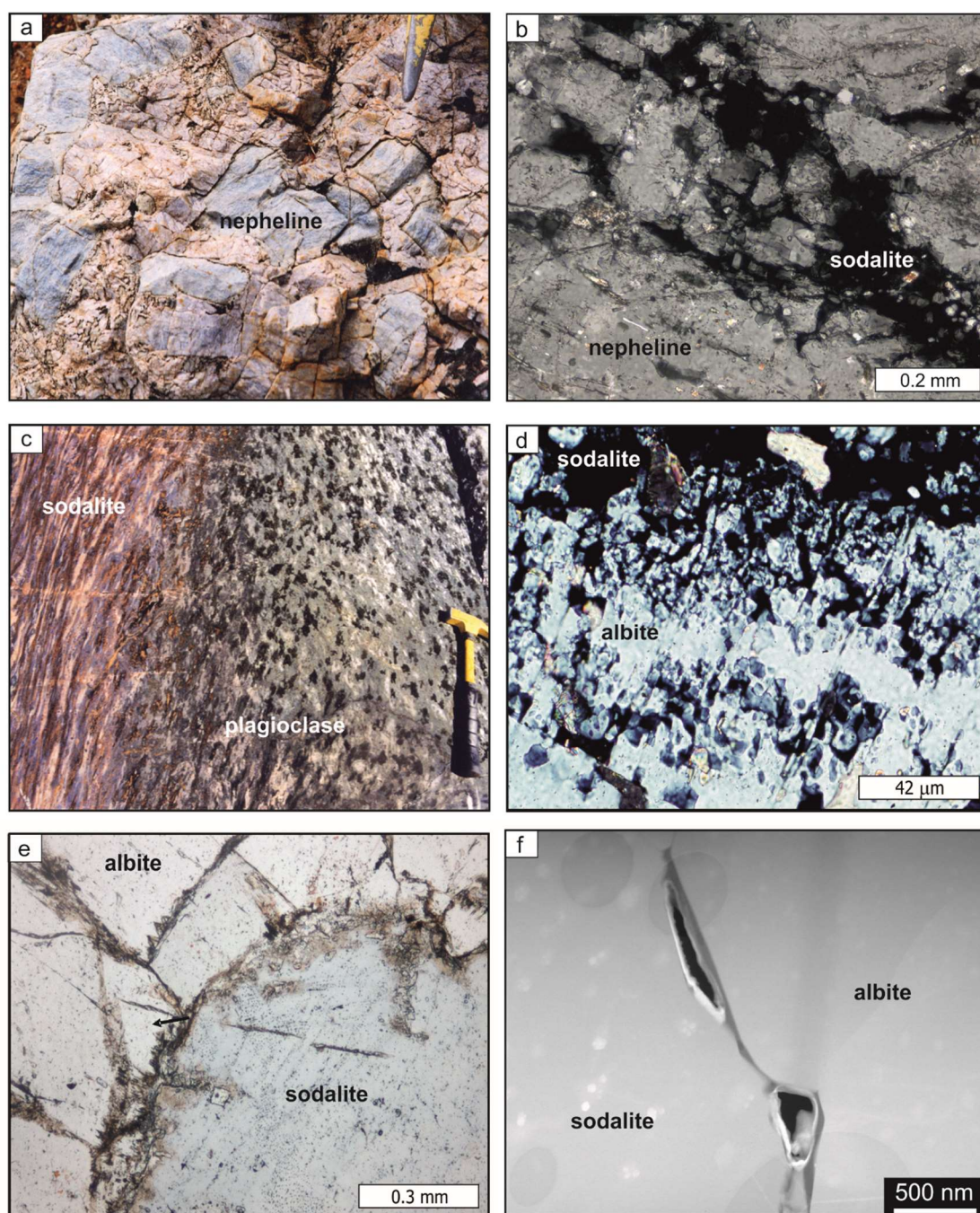
Figure 6. Natural examples of alkaline metasomatism in NW Namibia (**b**,**d**,**e**: microphotographs; **f**: TEM image); (**a**) Syenite direct contact to the carbonatite dykes contains euhedral nepheline of up to 15 cm across; (**b**) The pale blue tint of nepheline in (**a**) results from its partial replacement by sodalite along grain margins and irregular cracks; (**c**) Alkali-metasomatism of anorthosites, Namibia, is characterized by the replacement of plagioclase by sodalite; (**d**) Sodalite replaces albite along ist margins and the polysynthetic twin lamellae (sodalite isotropic); (**e**) Metasomatic sodalite of the natural rock samples from Namibia contains numerous fluid inclusions; (**f**) TEM-foil of the phase boundaries between albite and sodalite: an open channel is developed.

Sodalitization in the fenites starts along the grain margins of plagioclase and, if present, along cracks or albite twin lamellae (Figure 6c,d). The reaction fronts then progressively enter the plagioclase cores as embayed reaction zones. In most cases, replacement of plagioclase by sodalite went

to completion. The sodalite displays only minor porosity but fluid and secondary mineral inclusions, pointing to coarsening of a previously present microporosity (Figure 6e). The reaction interface between sodalite and albite, analyzed with TEM, is sharp and marked by an open channel (Figure 6f). Amorphous material was not observed but might have previously been present and then reacted to solid phases during long-term re-equilibration of the natural rock samples, in accordance with the interpretation of the amorphous material of our experiments as a metastable interstage product.

The major and trace element compositions of natural sodalite and plagioclase have been investigated with the aid of an electron microprobe and LA-ICPMS. Both sodalite and plagioclase are the almost pure sodium endmembers, generally displaying Fe_2O_3, CaO, K_2O, S and F contents <0.1 wt %. The REE contents of sodalite, determined by LA-ICPMS, are generally low (ΣREE: 2.5–3.3 ppm), whereas remarkably high values of As (422–657 ppm), Ti (38–57 ppm), Sn (14–51 ppm) and Ba (57–92 ppm) have been recorded. The Rb and Sr contents of sodalite are in the range of 9–13 ppm and 10–14 ppm, respectively. Regarding their REE patterns, all analyzed sodalites are characterized by an enrichment of the light REE (La_{cn}/Yb_{cn}: 4.6–12.1) and flattening in the heavy REE. All REE-patterns display a strong positive Eu anomaly (Eu_{cn}/Eu_{cn}^*: 1.5–3.3) although the CaO contents of sodalite are close to or below the detection limit. These REE patterns are similar to those obtained for plagioclase of the anorthosites, indicating that sodalite inherited its trace element budget from plagioclase.

4.4. Implications for the Reaction Process

In general, the observed reaction textures in the model system indicate an interfacial dissolution-precipitation mechanism, with the shape of the parent albite being preserved. In all experiments, cracks as well as grain and interphase boundaries act as preferred pathways for the aqueous solutions. The Si-rich and Na–Al-poor composition of the amorphous layer, developed as an intermediate metastable phase between the unaltered albite and the precipitating sodalite or nepheline, indicates that Al and Na went into the bulk solution during the early stage of the experiment. Since both sodalite and nepheline are subsequently nucleating and growing within the amorphous layer, aluminum has to be transported from the bulk fluid phase to the amorphous layer demonstrating that part of the γ-Al_2O_3 is dissolved and mobilized. The high porosity of the metastable amorphous material as well as the newly formed sodalite and nepheline allow for continuous transport of aqueous chemical reactants and products between the crystalline reaction front (release of Si, Al, Na) and the bulk fluid (H_2O, Na, Cl) (Figure 7). In case of sodalite, even fluid inclusions are frequent, providing evidence for excellent pathways for material transport via the fluid phase. In addition, the presence of open channels at the boundary between albite and the amorphous layer, containing precipitates of the circulating fluid, strongly suggest that the fluid permeated both the sodalite rims and the thick altered layer. The observed variable major element composition of the amorphous layer of different experiments is presumably mainly influenced by differences in the pH values of the bulk fluid, which underwent dramatic changes during the onset of sodalite crystallization (the composition of the educt phases, i.e., albite and γ-Al_2O_3, is almost similar with respect to the major element composition in all experiments). The formation of an amorphous layer as interstage product during the reaction process can moreover explain the observed behavior of the trace elements (i.e., inheritance of trace element patterns) during metasomatism. In situ LA-ICPMS analyses of the trace element contents of the educt albite and the product phases sodalite, nepheline and the amorphous phase indicate, that the alkaline metasomatism does not result in a complete equilibration and exchange between the solid phases involved in the reaction. Only minor compositional heterogeneities exist on the grain and sub-grain scale. The trace element budget of the product sodalite, nepheline and the amorphous phase is apparently inherited from the respective precursor albite. Due to its high viscosity when compared to the aqueous fluid, the amorphous material, containing the bulk trace element budget of the ancestor albite, remained fixed in position and underwent only minor exchange of trace elements with the circulating fluid. Following this, the composition of the metasomatic product phases provides direct

information about the precursor mineral and allows us to deduce the corresponding metasomatic reaction. Another possible explanation for the apparent lack of fractionation of any trace element during replacement may be the similarity in crystal structure of the reactants and products.
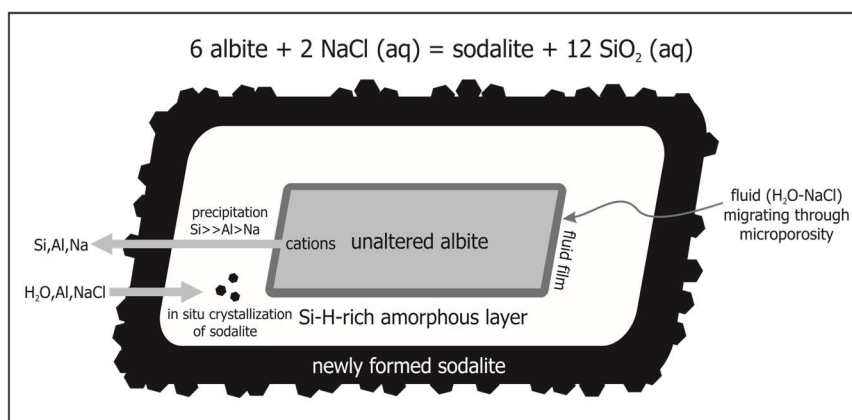

Figure 7. Model of transport mechanism for the hydrothermally driven reaction (Equation (1)): 6 albite + 2NaCl (aq) = sodalite + 12SiO$_2$ (aq).

The coupled interfacial dissolution–reprecipitation mechanism we observed, with amorphous material as a metastable interstage product, may be a more universal phenomenon. Amorphous altered layers are already described from a number of environments, i.e., among others, chemical weathering, radioactive waste storage, biomineralization, electrochemistry, and medical sciences, mostly related to low-T processes. Taken into account the high-T stability of the amorphous phase (up to 750 $^\circ$C) present in the early stages of the reaction process in our experiments this process may be a more universal process. Accordingly, results of our experiments bear important implications with respect to mineral replacement in the presence of a fluid in many geological environments, especially regarding the interpretation of trace element patterns and isotopic ratios of the product phases.

Conflicts of Interest: The authors declare no conflict of interest.

Appendix A

Table A1. Representative LA-ICPMS analyses of albite.

Sample	LT-05	LT-05	LT-05	LT-05	LT-04	LT-04	LT-04	LT-04	LT-04	HT-10	HT-10	33	34
					Swartb.					Lovozero		Lomnitz	
						ppm							
Li	7.79	5.28	<0.38	0.849	<0.37	<0.39	2.55	0.670	1.33	<0.38	<0.39	1.47	<0.37
Be	1.14	<0.58	0.981	<0.76	<0.93	<0.82	<0.74	<0.89	0.619	25.6	30.9	2.39	1.20
Ca	7169	2911	7174	7323	8763	8673	929	9019	8564	12.5	9.85	28.9	24.7
Sc	0.911	1.14	0.844	1.05	0.998	1.10	0.671	0.752	0.660	0.549	0.770	0.585	0.396
Ti	395	358	393	481	661	278	30.7	451	332	10.1	13.6	<4.7	<2.7
V	0.235	1.97	0.224	0.375	0.961	<0.15	0.124	0.204	<0.11	<0.12	<0.15	<0.23	<0.14
Cr	<2.1	<1.7	<2.4	<2.1	<2.2	<2.5	2.45	<2.3	<1.9	<2.9	<2.5	6.83	<2.1
Mn	19.2	13.2	25.7	42.6	45.8	11.2	2.21	22.5	21.7	10.5	17.3	3.84	<0.54
Co	0.309	0.102	0.862	0.543	0.761	0.188	<0.12	0.274	0.203	0.349	0.391	<0.22	<0.12
Ni	0.480	<0.35	1.05	1.85	1.09	<0.49	1.88	0.970	0.669	3.04	<0.62	<0.89	<0.43
Cu	3.13	5.15	3.65	3.49	3.34	3.73	13.1	3.41	3.60	13.8	6.92	14.8	5.50
Zn	4.89	<2.3	5.17	5.52	8.16	4.56	<2.8	6.13	4.71	13.7	<3.5	<4.9	<2.9
Ga	35.7	17.0	34.8	33.3	34.4	34.0	5.70	40.0	32.9	84.7	83.2	20.2	25.8
Rb	6.21	3.77	1.35	2.75	2.58	1.61	0.154	2.65	4.29	2.14	3.37	0.367	<0.06
Sr	1055	597	1054	1099	967	1007	101	1168	1168	5.97	6.79	7.61	18.5
Y	0.137	0.334	0.194	0.485	0.324	0.275	0.042	0.343	0.185	0.937	1.36	0.204	<0.03
Zr	<0.07	<0.06	<0.08	0.157	<0.08	<0.08	0.321	<0.10	<0.07	12.1	15.0	0.458	<0.07
Nb	<0.04	<0.03	<0.05	0.047	<0.04	<0.05	<0.03	<0.05	<0.03	1.11	1.31	0.625	<0.03
Sn	<0.37	0.466	<0.39	0.450	<0.39	0.432	<0.36	<0.43	0.617	<0.38	<0.41	<0.62	<0.37
Cs	<0.03	<0.03	<0.03	<0.03	<0.03	<0.05	<0.03	<0.03	<0.03	<0.04	<0.03	<0.07	<0.04
Ba	1043	311	711	581	776	641	21.8	1284	679	9.66	10.5	11.1	0.472
La	3.11	0.498	3.65	3.53	4.00	3.48	0.525	4.87	4.36	1.37	2.46	0.053	<0.03
Ce	5.28	0.980	6.03	6.45	6.88	6.99	0.926	7.95	7.43	3.14	5.14	0.144	<0.03
Pr	0.506	0.125	0.637	0.551	0.761	0.802	0.100	0.780	0.731	0.231	0.472	<0.05	<0.03
Nd	2.13	0.731	2.59	2.28	2.61	2.82	0.300	3.15	2.82	0.775	1.89	<0.34	<0.15
Sm	0.285	0.204	0.248	<0.23	0.489	0.310	<0.23	<0.27	0.207	<0.23	0.575	<0.41	<0.21
Eu	1.51	0.395	1.62	1.43	1.49	1.67	0.146	1.82	1.48	0.082	0.143	<0.11	<0.05
Gd	<0.21	<0.18	0.251	<0.19	0.319	0.261	<0.18	<0.31	<0.19	<0.23	<0.25	<0.41	<0.22
Tb	<0.03	0.036	<0.04	0.037	<0.04	<0.04	<0.03	<0.04	<0.03	0.043	<0.03	<0.05	<0.03
Dy	<0.15	<0.09	<0.15	0.215	<0.13	<0.19	<0.14	<0.17	<0.13	<0.17	0.383	<0.33	<0.13
Ho	<0.03	<0.03	<0.03	<0.03	<0.04	<0.04	<0.04	<0.04	<0.03	<0.04	0.040	<0.06	<0.03
Er	<0.09	<0.09	<0.11	<0.12	<0.11	<0.11	<0.11	<0.13	<0.09	<0.12	<0.11	<0.18	<0.11
Tm	<0.03	<0.03	<0.04	<0.03	<0.04	<0.04	<0.04	<0.05	<0.03	<0.04	<0.03	<0.04	<0.03
Yb	<0.17	<0.14	<0.16	<0.19	<0.18	<0.21	<0.18	<0.21	<0.17	<0.19	<0.19	<0.28	<0.16
Lu	<0.04	<0.03	<0.04	<0.03	<0.03	<0.05	<0.03	<0.04	<0.03	<0.05	0.049	<0.07	<0.03
Hf	<0.11	<0.11	<0.11	<0.13	<0.14	<0.14	<0.13	<0.16	<0.11	<0.14	<0.14	<0.24	<0.13
Ta	<0.02	<0.03	<0.03	<0.03	<0.03	<0.04	0.075	<0.04	<0.03	0.091	0.137	0.145	<0.03
Pb	3.61	1.95	4.00	4.68	3.48	2.84	3.96	5.94	5.86	1.02	0.266	1.21	<0.09
Th	<0.06	<0.04	<0.05	<0.05	<0.06	<0.06	<0.05	<0.06	<0.06	0.976	1.65	<0.09	<0.04
U	<0.04	<0.04	<0.05	<0.05	<0.05	<0.06	<0.05	<0.06	<0.04	0.255	0.238	<0.09	<0.05

Table A2. Representative LA-ICPMS analyses of sodalite, nepheline, and the amorphous phase.

Sample	LT-05	LT-05	LT-05	LT-05	LT-04	LT-04	LT-04	HT-08	HT-08	HT-08	HT-10	HT-10	33	34	34
				Swartbooisdrif						Lovozero				Lomnitz	
	Sdl	Sdl	Sdl	Sdl	Sdl	Sdl	Sdl	Sdl	am	am	Sdl	Sdl	Sdl	Sdl	Nph
								ppm							
Li	<0.32	0.867	0.989	7.53	2.55	0.594	1.20	31.4	2.25	2.31	<0.48	2.10	0.834	0.720	0.972
Be	<0.69	<0.58	<1.2	<0.88	<0.74	<0.55	<0.66	2.34	<0.21	<0.23	<0.88	<0.38	3.99	<0.82	<1.1
Ca	87.6	513	2535	2315	929	1122	310	121	2324	2364	19.4	2466	26.1	11.6	67.6
Sc	0.385	0.756	0.960	0.943	0.671	0.462	0.391	0.327	0.501	0.442	0.592	0.449	0.454	0.521	0.477
Ti	7.82	111	130	239	30.7	4.44	5.81	40.8	66.0	71.5	<4.2	74.1	<5.4	<4.5	<3.9
V	<0.12	<0.15	0.392	1.23	0.124	<0.11	<0.11	1.78	0.389	0.415	0.274	0.483	0.344	0.232	<0.16
Cr	<2.1	<2.4	7.05	<2.9	2.45	<1.6	<1.7	<4.1	<0.68	<0.65	<2.8	1.13	<3.4	14.5	<2.9
Mn	0.464	2.57	13.4	18.6	2.21	1.23	<0.36	28.0	6.91	7.18	2.14	6.74	4.26	<0.87	<0.84
Co	<0.11	<0.13	0.514	0.875	<0.12	<0.07	0.162	0.549	0.064	0.106	<0.15	<0.06	<0.23	<0.12	<0.18
Ni	<0.46	0.607	6.34	4.97	1.88	0.649	<0.46	9.21	0.365	0.307	4.42	1.04	0.943	0.763	<0.63
Cu	16.0	15.1	16.4	20.9	13.1	8.43	12.2	59.4	4.57	4.60	25.4	7.27	10.4	13.6	15.2
Zn	<2.9	<2.9	5.93	4.83	<2.8	2.40	<2.6	77.1	5.20	4.01	<3.9	8.81	9.58	<3.2	<3.8
Ga	5.15	5.85	15.0	14.8	5.70	9.42	3.60	9.80	1.96	1.93	3.05	1.67	26.6	4.26	7.89
Rb	<0.06	<0.07	0.690	0.582	0.154	0.080	<0.06	2.44	16.9	16.8	2.12	16.3	0.396	0.164	1.20
Sr	6.20	57.4	411	382	101	174	18.9	10.6	19.2	19.4	1.23	20.9	5.11	0.260	29.7
Y	<0.04	0.208	0.249	0.319	0.042	0.062	0.040	0.248	0.718	0.736	<0.04	0.871	0.610	0.378	0.056
Zr	<0.07	0.187	<0.12	1.43	0.321	<0.06	<0.07	3.14	52.0	51.1	0.341	60.6	1.77	1.16	0.158
Nb	0.098	3.03	0.523	3.88	<0.03	<0.03	<0.04	7.74	0.219	0.244	0.191	0.190	1.72	11.4	0.122
Sn	1.05	0.457	<0.54	<0.52	<0.36	0.340	<0.34	2.63	0.270	0.196	0.487	0.453	0.682	<0.39	<0.49
Cs	<0.05	<0.03	<0.06	<0.05	<0.03	<0.03	<0.03	<0.08	0.164	0.193	<0.04	0.175	0.056	<0.04	<0.06
Ba	8.15	10.4	145	113	21.8	64.3	2.95	24.1	116	120	1.58	130	15.3	1.21	94.2
La	0.123	0.906	15.1	6.85	0.525	0.806	0.088	0.749	0.972	0.907	0.072	1.07	0.066	<0.04	<0.04
Ce	0.060	1.04	4.31	6.97	0.926	0.712	0.070	1.05	1.66	1.64	0.129	1.80	0.294	<0.04	<0.04
Pr	<0.03	0.103	0.449	0.813	0.100	0.070	<0.02	0.143	0.179	0.189	<0.03	0.159	<0.05	<0.03	<0.03
Nd	<0.18	0.466	1.5	3.39	0.300	0.273	<0.14	0.663	0.636	0.656	<0.24	0.636	<0.28	<0.19	<0.26
Sm	<0.23	<0.25	<0.35	0.214	<0.23	<0.21	<0.22	0.139	0.138	0.109	<0.27	0.256	<0.32	<0.22	<0.35
Eu	<0.06	0.251	0.736	1.39	0.146	0.057	<0.05	<0.14	0.090	0.095	<0.08	0.035	<0.08	<0.06	<0.09
Gd	<0.19	<0.21	<0.39	<0.24	<0.18	<0.16	<0.21	<0.39	0.127	0.102	<0.28	0.099	<0.29	<0.23	<0.26
Tb	<0.03	<0.03	<0.06	<0.04	<0.03	<0.02	<0.03	<0.06	0.016	0.022	<0.04	0.014	<0.05	<0.03	<0.04
Dy	<0.15	<0.16	<0.21	<0.16	<0.14	<0.11	<0.14	<0.22	0.121	0.080	<0.18	0.158	<0.21	<0.15	<0.16
Ho	<0.03	<0.04	<0.05	<0.05	<0.04	<0.03	<0.03	<0.08	0.021	0.034	<0.03	0.030	<0.04	<0.03	<0.05
Er	<0.11	<0.09	<0.17	<0.12	<0.11	<0.08	<0.08	<0.19	0.092	0.065	<0.13	0.082	<0.17	<0.12	<0.14
Tm	<0.03	<0.04	<0.06	<0.05	<0.04	<0.03	<0.03	<0.07	<0.01	0.017	<0.04	0.016	<0.05	<0.04	<0.04
Yb	<0.16	<0.18	<0.22	<0.24	<0.18	<0.13	<0.17	<0.29	0.116	<0.06	<0.24	0.106	<0.24	<0.16	<0.22
Lu	<0.05	<0.03	<0.05	<0.05	<0.03	<0.03	<0.03	<0.08	<0.01	0.013	<0.04	<0.02	<0.05	<0.03	<0.05
Hf	<0.12	<0.12	<0.21	<0.19	<0.13	<0.09	<0.12	<0.27	1.22	1.36	<0.18	1.65	<0.21	<0.15	<0.17
Ta	<0.03	1.23	0.158	2.21	0.075	<0.02	<0.04	0.098	0.013	0.027	<0.04	<0.02	0.198	0.193	<0.03
Pb	5.75	3.52	56.2	61.0	3.96	5.25	1.10	17.8	3.78	3.82	2.94	4.81	1.55	0.846	1.76
Th	<0.05	<0.06	0.158	<0.07	<0.05	<0.04	<0.05	<0.11	0.230	0.230	<0.07	0.325	<0.07	0.085	<0.07
U	<0.05	<0.04	0.155	<0.07	<0.05	<0.04	<0.04	<0.11	0.155	0.145	<0.06	0.157	<0.07	<0.05	<0.07

(am = amorphous phase; Nph = nepheline; Sdl = sodalite).

References

1. Merino, E.; Wang, Y.; Wang, Y.; Nahon, D. Implications of pseudomorphic replacement for reaction–transport modelling in rocks. *Mineral. Mag.* **1994**, *58*, 599–601. [CrossRef]
2. Merino, E.; Dewers, T. Implications of replacement for reaction–transport modelling. *J. Hydrol.* **1998**, *209*, 137–146. [CrossRef]
3. Cesare, B. Multi-stage pseudomorphic replacement of garnet during polymetamorphism: 1. Microstructures and their interpretation. *J. Metamorph. Geol.* **1999**, *17*, 723–734. [CrossRef]
4. Putnis, A. Mineral replacement reactions: From macroscopic observations to microscopic mechanisms. *Mineral. Mag.* **2002**, *66*, 689–708. [CrossRef]
5. Putnis, C.V.; Mezger, K. A mechanism of mineral replacement: Isotope tracing in the model system KCl–KBr–H_2O. *Geochim. Cosmochim. Acta* **2004**, *68*, 2839–2848. [CrossRef]
6. Putnis, A. Mineral replacement reactions. *Rev. Mineral. Geochem.* **2009**, *70*, 87–124. [CrossRef]
7. Walker, F.D.L.; Lee, M.R.; Parsons, I. Micropores and micropermeable texture in alkali feldspars: Geochemical and geophysical implications. *Mineral. Mag.* **1995**, *59*, 507–536. [CrossRef]
8. Putnis, A.; Mauthe, G. The effect of pore size on cementation in porous rocks. *Geofluids* **2001**, *1*, 37–41. [CrossRef]
9. Finch, A.A. Conversion of nepheline to sodalite during subsolidus processes in alkaline rocks. *Mineral. Mag.* **1991**, *55*, 459–463. [CrossRef]
10. Sharp, Z.D.; Helffrich, G.R.; Bohlen, S.R.; Essene, E.J. The stability of sodalite in the system $NaA1SiO_4$-NaCI. *Geochim. Cosmochim. Acta* **1989**, *53*, 1943–1954. [CrossRef]
11. Balassone, G.; Bellatreccia, F.; Mormone, A.; Biagioni, C.; Pasero, M.; Petti, C.; Mondillo, N.; Fameli, G. Sodalite-group minerals from the Somma-Vesuvius volcanic complex, Italy: A case study of K-feldspar-rich xenoliths. *Mineral. Mag.* **2012**, *76*, 191–212. [CrossRef]
12. Upadhyay, D. Alteration of plagioclase to nepheline in the Khariar alkaline complex, SE India: Constraints on metasomatic replacement reaction mechanisms. *Lithos* **2012**, *155*, 19–29. [CrossRef]
13. Dumańska-Słowik, M.; Heflik, W.; Pieczka, A.; Sikorska, M.; Dąbrowa, Ł. The transformation of nepheline and albite into sodalite in pegmatitic mariupolite of the Oktiabrski Massif (SE Ukraine). *Spectrochim. Acta Part A Mol. Biomol. Spectrosc.* **2015**, *150*, 837–845. [CrossRef] [PubMed]
14. Kotelnikov, A.; Zhornyak, L. Stability of sodalite under hydrothermal conditions. *Geochem. Int.* **1995**, *32*, 87–90.
15. Pearce, N.J.G.; Perkins, W.T.; Westgate, J.A.; Gorton, M.P.; Jackson, S.E.; Neal, C.R.; Chenery, S.P. A compilation of new and published major and trace element data for NIST SRM 610 and NIST SRM 612 glass reference materials. *Geostand. Newslett. J. Geostand. Geoanal.* **2007**, *21*, 115–144. [CrossRef]
16. Wirth, R. Focused Ion Beam (FIB): A novel technology for advanced application of micro– and nanoanalysis in geosciences and applied mineralogy. *Eur. J. Mineral.* **2004**, *16*, 863–877. [CrossRef]
17. Wirth, R. Focused Ion Beam (FIB) combined with SEM and TEM: Advanced analytical tools for studies of chemical composition, microstructure and crystal structure in geomaterials on a nanometre scale. *Chem. Geol.* **2009**, *261*, 217–229. [CrossRef]
18. Drüppel, K.; Hoefs, J.; Okrusch, M. Fenitizing processes induced by ferrocarbonatite magmatism at Swartbooisdrif, NW Namibia. *J. Petrol.* **2005**, *46*, 377–406. [CrossRef]
19. Drüppel, K. Petrogenesis of the Mesoproterozoic Anorthosite, Syenite and Carbonatite Suites of NW Namibia and Their Contribution to the Metasomatic Formation of the Swartbooisdrif Sodalite Deposits. Ph.D. Thesis, University of Würzburg, Würzburg, Germany, 2003.
20. Nesbitt, H.W.; Muir, I.J. SIMS depth profiles of weathered plagioclase and processes affecting dissolved Al and Si in some acidic soil solutions. *Nature* **1988**, *334*, 336–338. [CrossRef]
21. Casey, W.H.; Westrich, H.R.; Arnold, G.W.; Banfield, J.E. The surface chemistry of dissolving labradorite feldspar. *Geochim. Cosmochim. Acta* **1989**, *53*, 821–832. [CrossRef]
22. Hellmann, R.; Dran, J.-C.; Della Mea, G. The albite–water system Part III. Characterization of leached and hydrogen–enriched layers formed at 300 °C using MeV ion beam techniques. *Geochim. Cosmochim. Acta* **1997**, *61*, 1575–1594. [CrossRef]
23. Schweda, P.; Sjöberg, L.; Södervall, U. Near–surface composition of acid–leached labradorite investigated by SIMS. *Geochim. Cosmochim. Acta* **1997**, *61*, 1985–1994. [CrossRef]

24. Hellmann, R.; Penisson, J.M.; Hervig, R.L.; Thomassin, J.H.; Abrioux, M.F. An EFTEM/HRTEM high–resolution study of the near surface of labradorite feldspar altered at acid pH: Evidence for interfacial dissolution–reprecipitation. *Phys. Chem. Miner.* **2003**, *30*, 192–197. [CrossRef]

25. Weissbart, E.J.; Rimstidt, J.D. Wollastonite incongruent dissolution and leached layer formation. *Geochim. Cosmochim. Acta* **2000**, *64*, 4007–4016. [CrossRef]

26. Labotka, T.C.; Cole, D.R.; Fayek, M.; Riciputi, L.R.; Stadermann, F.J. Coupled cation and oxygen–isotope exchange between alkali feldspar and aqueous chloride solution. *Am. Mineral.* **2004**, *89*, 1822–1825. [CrossRef]

27. Hellmann, R.; Wirth, R.; Daval, D.; Barnes, J.-P.; Penisson, J.-M.; Tisserand, D.; Epicier, T.; Florin, B.; Hervig, R.L. Unifying natural and laboratory chemical weathering with interfacial dissolution–reprecipitation: A study based on nanometer–scale chemistry of fluid–silicate interfaces. *Chem. Geol.* **2012**, *294–295*, 203–216. [CrossRef]